Acta Crystallographica Section B
Structural Science
ISSN 0108-7681

Structures of two new high-pressure forms of $AlPO_4$ by X-ray powder diffraction and NMR spectroscopy

Masami Kanzaki,[a]* Xianyu Xue,[a] Sindy Reibstein,[b]‡ Eleanor Berryman[c] and Seonyi Namgung[d]

[a]Institute for Study of the Earth's Interior, Okayama University, 827 Yamada, Misasa, Tottori 682-0193, Japan, [b]Faculty of Geosciences, Geoengineering and Mining, Institute of Mineralogy, Technische Universität Bergakademie Freiberg, 09599 Frieberg, Germany, [c]Department of Earth and Planetary Sciences, McGill University, Frank Dawson Adams, 3450 University Street, Montreal, Quebec, Canada H3A 2A7, and [d]Department of Earth System Sciences, Yonsei University, Seodaemun, Shinchon 134, Seoul 120-749, Korea

‡ Current address: Department of Materials Science, University of Erlangen-Nuremberg, 91058 Erlangen, Germany.

Correspondence e-mail: mkanzaki@misasa.okayama-u.ac.jp

Received 24 July 2010
Accepted 6 December 2010

The crystal structures of two new high-pressure $AlPO_4$ phases are reported. One phase synthesized at 6 GPa and 1523 K is triclinic ($P\bar{1}$) whilst the other phase synthesized at 7 GPa and 1773 K is monoclinic ($P2_1/c$). ^{31}P MAS (magic-angle spinning) NMR suggests three tetrahedral P sites with equal abundance in both phases. ^{27}Al 3Q MAS NMR spectra provided evidence for two octahedral sites and one five-coordinated Al site in each phase. The crystal structures were solved using an *ab initio* structure determination technique from synchrotron powder X-ray diffraction data utilizing the local structural information from NMR, and were further refined by the Rietveld method. Both phases contain doubly bent chains made of six edge-shared Al polyhedra (including five-coordinated Al), which are joined by PO_4 tetrahedra. The $P\bar{1}$ phase is isostructural with $FeVO_4$ and $AlVO_4$. The two phases differ in the packing manner of the chains. This study has demonstrated that the combined application of *ab initio* structure determination *via* X-ray powder diffraction and solid-state NMR spectroscopy is a powerful approach to the rapid solution of complex inorganic crystal structures.

1. Introduction

$AlPO_4$ is isoelectronic to SiO_2 and adapts a structure (berlinite) analogous to α-quartz at ambient pressure (Sharan & Dutta, 1964). Kruger & Jeanloz (1990) first reported pressure-induced amorphization of berlinite. Similar behavior is also known for quartz and other tetrahedral network structures (*e.g.* Hemley *et al.*, 1988). However, unlike other materials, the amorphized berlinite was reported to revert to a crystalline state again when pressure is released. This peculiar behavior has attracted much attention, and was termed 'memory glass' (Kruger & Jeanloz, 1990). Subsequently, X-ray diffraction and Raman spectroscopic studies of berlinite under pressure were conducted using diamond–anvil cell (DAC) high-pressure devices. A phase transition from berlinite to a poorly crystalline phase was observed (*e.g.* Gillet *et al.*, 1995; Sharma *et al.*, 2000; Pellicer-Porres *et al.*, 2007). The transition was found to be reversible and could account for the previously reported 'memory glass' behavior. These studies have revealed the following pressure-induced phase transition sequence for $AlPO_4$: berlinite to $CrVO_4$-structured phase (space group *Cmcm*) at around 13 GPa (Gillet *et al.*, 1995; Sharma *et al.*, 2000), and the *Cmcm* phase to distorted $CaCl_2$ structure at $\sim$ 60 GPa (Pellicer-Porres *et al.*, 2007). Accompanying these transitions the oxygen coordination numbers of Al and P increase from all 4 in berlinite, to 6 for Al and 4 for P in the *Cmcm* phase, and to all 6 in the distorted $CaCl_2$ phase. All of

these studies were, however, conducted at ambient temperature and thus the observed transition sequence might not reflect the state of thermodynamic equilibrium. Indeed, early high-pressure and high-temperature studies in this system based on quench experiments reported several unknown phases at 6–7 GPa. Dachille & Roy (1959) reported the transition from berlinite to a new phase at 6 GPa and 773 K, although no details of the phase were given. Seifert (1968) reported three new phases: HI, HII and HIII. The HI and HII phases were observed at 6 GPa and 1173 K, and the HIII phase was observed at 7–10 GPa and 1173–1273 K. The HIII phase was identified as isostructural to $CrVO_4$ (*Cmcm*), but no structural information for the HI and HII phases was given. Very recently, the synthesis of the $CrVO_4$ phase of $AlPO_4$ at 18 GPa and 1948 K was reported (Stebbins *et al.*, 2009).

To clarify the phase relations in this system, we recently carried out high-pressure and high-temperature experiments at 6–7 GPa and 1273–1773 K, and found two unknown $AlPO_4$ phases: a triclinic phase ($P\bar{1}$) at 6 GPa and 1273–1523 K, and a monoclinic phase ($P2_1/c$) at 6–7 GPa and 1773 K. Here we report the crystal structures for both phases determined by combined synchrotron powder X-ray diffraction and high-resolution ^{31}P magic-angle spinning (MAS) and ^{27}Al triple-quantum (3Q) MAS nuclear magnetic resonance (NMR) spectroscopy. More detailed NMR spectroscopic studies on these phases utilizing various two-dimensional through-space (dipolar) and through-bond (scalar, *J* coupled) ^{31}P–^{31}P and ^{27}Al–^{31}P correlation techniques (that enabled unambiguous assignment of all the ^{31}P and ^{27}Al NMR peaks) are reported separately (Xue & Kanzaki, 2010, 2011).

2. Experimental methods

2.1. Sample synthesis and descriptions

A number of high-pressure $AlPO_4$ samples have been synthesized at 6–7 GPa and 1273–1773 K using multi-anvil apparatus at either the Institute for Study of the Earth's Interior (ISEI) or the beamline BL04B1 of SPring-8. The recovered samples were examined under an optical microscope, and the phases were identified by micro-Raman spectroscopy, detailed ^1H, ^{31}P and ^{27}Al NMR spectroscopy and X-ray powder diffraction. Selected samples were also analyzed with an electron microprobe.

Only the synthesis procedure for two samples (#080927B and #081113, one for each $AlPO_4$ phase) that were subjected to synchrotron X-ray powder diffraction will be described in detail here, although all the other samples give consistent results and will be described where necessary. The two samples were produced using a Kawai-type double-stage multi-anvil system (SPEED1500) at beamline BL04B1 of SPring-8 (see Utsumi *et al.*, 1998). The starting material was a reagent-grade $AlPO_4$ (> 98% purity, purchased from Sigma Chemical Co.) that was dried at 1273 K for 28 h before loading and sealing in a 3.0 mm outer diameter Pt capsule. The length of the Pt tube was $\sim$ 3.5 mm after sealing and squeezing to fit into the high-pressure cell. A Cr-doped MgO octahedral pressure cell assembly (18 *M* cell; edge length 18 mm) was employed. Pressure was estimated from a pressure calibration curve constructed from an *in-situ* X-ray diffraction study with the same pressure cell (Kanzaki, unpublished) with an uncertainty of less than 0.5 GPa. A $W_{97}Re_3$–$W_{75}Re_{25}$ thermocouple was used to measure temperature with fluctuations to less than 2 K. A stepped graphite tube heater was employed to minimize the temperature gradient in the sample (Kanzaki, 1992).

Sample #080927B was synthesized at 6 GPa and 1523 K for 1 h. It was well sintered with grain sizes of a few μm, and was composed predominantly of an unknown $AlPO_4$ phase with minor trolleite ($Al_4(OH)_3[PO_4]_3$), corundum (Al_2O_3) and unidentified phosphate phase(s) (see details below). The presence of trolleite indicates that the starting material contained a small amount of water. Our preliminary experiments conducted at 6 GPa and 1273 K (#080707) to 1773 K (#080709) during the early stages of this study (MISIP 2008) using undried $AlPO_4$ chemical as the starting material (containing about 2 wt % H_2O, as determined by quantitative ^1H MAS NMR measurement) resulted in more abundant trolleite, coexisting with a dominant $AlPO_4$ phase, as revealed by micro-Raman, and detailed ^1H, ^{31}P and ^{27}Al NMR measurements. Trolleite has a unique dense structure consisting of Al octahedral face-sharing dimers that link to one another by corner-sharing OH groups to form infinite double chains, which are bridged together by PO_4 tetrahedra to form a three-dimensional structure (Moore & Araki, 1974). It has been previously reported to be stable up to at least 2.35 GPa and 1273 K (Bass & Sclar, 1979). Our observation of this phase from samples recovered from 6 GPa and 1273–1773 K further extended its stability field to higher pressure.

Sample #081113 was synthesized at 7 GPa and 1773 K for 1 h. It was coarse grained with crystal sizes of a few tens of μm, and was mainly composed of an unknown $AlPO_4$ phase (different from above) with minor corundum, as confirmed by NMR and X-ray powder diffraction (see below).

Although the chemical compositions of the two samples described above have not been analyzed, chemical analysis and mapping have been performed on another sample (#080709) synthesized at 6 GPa and 1773 K for 1 h. The latter was produced using a 5000 ton Kawai-type double-stage uniaxial split-sphere multi-anvil press at ISEI using undried $AlPO_4$ as mentioned above. Detailed micro-Raman and ^1H, ^{31}P and ^{27}Al NMR measurements revealed that the sample consisted predominantly of a large-grained $AlPO_4$ phase (with crystal sizes of a few tens of μm) that also occurs in sample #081113 (7 GPa and 1773 K), with minor smaller grains of trolleite and corundum. The chemical analysis was made on selected grains (mounted in epoxy resin and polished) using a Jeol JXA-8800 electron microprobe with an accelerating voltage of 10 kV, a beam current of 20 nA and a beam diameter of 2 μm. The average composition for ten analyses on the main $AlPO_4$ phase gives: 41.36 (0.25) wt % Al_2O_3, 59.96 (0.70) wt % P_2O_5 and 101.32 (0.84) wt % total with an Al/P atomic ratio of 0.96 (0.01), within uncertainty of that expected for the ideal $AlPO_4$ composition. Analysis for samples synthesized at 6 GPa and lower temperatures (1273–

Table 1
Experimental details.

For all structures: $AlPO_4$, M_r = 121.95. Experiments were carried out at 300 K with synchrotron radiation, λ = 1.00036 Å using a Debye–Scherrer diffractometer. Refinement was with 0 restraints.

	$P\bar{1}$	$P2_1/c$
Crystal data		
Crystal system, space group	Triclinic, $P\bar{1}$	Monoclinic, $P2_1/c$
a, b, c (Å)	6.1328 (1), 7.5151 (1), 8.5801 (1)	6.13219 (6), 14.3465 (1), 8.57620 (9)
α, β, γ (°)	98.2630 (7), 104.6220 (8), 102.1398 (8)	90, 104.7426 (5), 90
V (Å^3)	365.9 (1)	729.7 (1)
Z	6	12
μ (mm^{-1})	3.24	3.25
Specimen shape, size (mm)	Cylinder, 3.0 × 0.3	Cylinder, 3.0 × 0.3
Data collection		
Specimen mounting	Capillary	Capillary
Data collection mode	Transmission	Transmission
Scan method	Step	Step
2θ values (°)	$2\theta_{min}$ = 5.91, $2\theta_{max}$ = 76.99, $2\theta_{step}$ = 0.01	$2\theta_{min}$ = 7.01, $2\theta_{max}$ = 77.49, $2\theta_{step}$ = 0.01
Refinement		
R factors and goodness of fit	R_p = 0.033, R_{wp} = 0.045, R_{exp} = 0.031, R_{Bragg} = 0.017, χ^2 = 2.045	R_p = 0.036, R_{wp} = 0.049, R_{exp} = 0.031, R_{Bragg} = 0.021, χ^2 = 2.403
No. of data points	6886	7049
No. of parameters	130	145

Computer programs: *FOX* (Favre-Nicolin & Černý, 2002), *RIETAN-FP* (Izumi & Momma, 2007), *VESTA* (Momma & Izumi, 2008).

1523 K, containing the other $AlPO_4$ phase) was difficult because of fine grain sizes. Nevertheless, the dominant phase in these samples has been found to be isostructural with $AlVO_4$ and $FeVO_4$ (see details below) and it is reasonable to assume that it also has an $AlPO_4$ composition.

All previous synthesis studies of the $AlPO_4$ system have been conducted below 1273 K (Dachille & Roy, 1959; Seifert, 1968). Therefore, the phase observed at 6–7 GPa and 1773 K is likely a new phase not reported thus far. The other phase obtained at 6 GPa and 1523 K also occurs in samples synthesized at 6 GPa and 1273 K (*e.g.* #080707) in our preliminary experiments. It could thus correspond to one of the phases reported at 6 GPa and 773–1173 K in previous studies (Dachille & Roy, 1959; Seifert, 1968), although no X-ray diffraction, spectroscopic or chemical data for the latter are available for comparison. It is also worth pointing out that one of the latter phases (especially the coexisting phases reported in Seifert, 1968) could also correspond to the hydrous phase, trolleite, because of the hygroscopic nature of the system and the observation of trolleite in our experiments in the nominally anhydrous $AlPO_4$ system.

2.2. NMR spectroscopy

All the NMR spectra were obtained using a Varian Unity-Inova 400 MHz (9.4 T) spectrometer and a 1.6 mm Varian T3 MAS NMR probe at a resonance frequency of 400.4, 162.1 and 104.3 MHz for ^{1}H, ^{31}P and ^{27}Al. The ^{1}H chemical shift was externally referenced to tetramethylsilane (TMS); the ^{27}Al chemical shift was referenced to a 1 *M* $Al(NO_3)_3$ aqueous solution; the ^{31}P chemical shift was referenced to an 85% H_3PO_4 aqueous solution using solid $(NH_4)_2HPO_4$ as a secondary standard (1.33 p.p.m. relative to 85% H_3PO_4). All the chemical shifts were reproducible to better than ± 0.1 p.p.m.

The ^{31}P MAS NMR spectra have been acquired at a spinning rate of 30 kHz with a spectral width of 100 kHz, a $\pi/2$ pulse of 2.2 µs and a recycle delay of 700 s (#080927B) and 400 s (#081113) (both $> 5\,T_1$, T_1: spin-lattice relaxation time constant) to ensure quantitative results. No decoupling was applied during acquisition.

The ^{27}Al MAS NMR spectra have been acquired at a spinning rate of 30 kHz with a spectral width of 2 MHz, a pulse of 0.5 µs (∼ 30° tip angle for selective central transition) and a recycle delay time of 3 s. No decoupling was applied during acquisition. Since ^{27}Al MAS NMR spectra are often broadened by second-order quadrupolar coupling, high-resolution two-dimensional ^{27}Al triple-quantum (3Q) MAS NMR spectra were also obtained using the three-pulse z-filter sequence (without decoupling) described by Amoureux, Fernandez & Steuernagel (1996). The optimized lengths (with an RF field of 208 kHz) for the 3Q excitation and 3Q → 0Q reconversion pulses were 2 and 0.7 µs, respectively, and the length of the third soft z-filter $\pi/2$ pulse was 11 µs. A delay of 20 µs was kept between the last two pulses. The Sates–Haberkorn–Ruben (hypercomplex) method was used to achieve quadrature detection in the 3Q evolution period, t_1. Shearing and chemical shift reference in the isotropic ($F1$) dimension follow the convention of Amoureux & Fernandez (1998). Simulations of the one-dimensional ^{27}Al MAS NMR spectra and the MAS ($F2$) cross sections of two-dimensional 3Q MAS NMR spectra have been performed with the STARS software (Varian Inc.).

In order to assist phase identification/peak assignment, one-dimensional cross-polarization (CP) MAS NMR and two-dimensional (dipolar, CP-based) heteronuclear correlation (HETCOR) experiments have been performed for several pairs of nuclei (^{1}H–^{27}Al, ^{1}H–^{31}P, ^{27}Al–^{31}P), mostly at a spinning rate of 30 kHz. Furthermore, high-resolution two-dimensional (dipolar) ^{27}Al–^{31}P 3Q-HETCOR spectra (that correlate the ^{27}Al isotropic dimension with the ^{31}P MAS dimension) have also been obtained. Details of such experiments are reported in Xue & Kanzaki (2009, 2010, 2011); see also the supplementary material.[1]

[1] Supplementary data for this paper are available from the IUCr electronic archives (Reference: WH5011). Services for accessing these data are described at the back of the journal.

Table 2
^{31}P NMR results.

Phase(s)	P site†	δ_i^P (p.p.m.)	FWHM (p.p.m.)‡	T_1^P (s)
#080927B (6 GPa, 1523 K)				
$AlPO_4$	P2	−18.7	1.0	83 (5)
($P\bar{1}$)	P1	−27.7	1.2	96 (6)
	P3	−39.4	1.8	126 (10)
Trolleite	P1	−29.3		
	P2	−32.9		
Unknown		−15		
Unknown		−24		
Unknown		−31		
#081113 (7 GPa, 1773 K)				
$AlPO_4$	P2	−17.1	0.9	32 (1)
($P2_1/c$)	P1	−26.7	1.2	57 (3)
	P3	−39.8	1.8	70 (5)

† Site numbering corresponds to that for crystallographic sites, and is assigned according to two-dimensional through-bond ^{31}P–^{31}P homonuclear correlation (INADEQUATE) and ^{27}Al–^{31}P heteronuclear correlation (3Q-J-HETCOR) experiments for the $AlPO_4$ phases (see Xue & Kanzaki, 2010, 2011), and according to the relative abundances (P1:P2 = 1:2) for trolleite (Moore & Araki, 1974). ‡ FWHM at a spinning rate of 30 kHz and a magnetic field of 9.4 T without decoupling during acquisition.

2.3. X-ray powder diffraction

Synchrotron powder X-ray diffraction data at ambient conditions were obtained at the beamline BL19B2 of SPring-8. A large Debye–Scherrer camera with an imaging plate detector was used (Nishibori *et al.*, 2001). The measurement procedure is identical to that reported in Kanzaki (2010). The detector covers a 2θ range of 0–80° with an angle resolution of 0.01°. Each sample was crushed in an agate mortar, and a portion of less than 1 mg of the powdered sample was loaded into a borosilicate glass capillary with 0.3 mm outer diameter. The capillary tube was rotated during the measurement to reduce the effect of preferred orientation. The exposure time for each sample was 10 min. The wavelength of the X-ray beam used was 1.00036 Å as calibrated by the NIST standard CeO_2 measured under the same conditions. The measurement conditions are summarized in Table 1.

The diffraction patterns of the two phases were indexed using *TREOR*90 (Werner *et al.*, 1985). The crystal structures of the two phases were solved using the *ab initio* structure determination program *FOX* (Favre-Nicolin & Černý, 2002), which employs a real-space searching with parallel tempering optimization algorithm. The program randomly moves and rotates atoms and user-defined polyhedra in real space and calculates its corresponding powder diffraction pattern. It then compares the calculated pattern with that observed. By using parallel tempering, the program searches for the best structure that reproduces the observed diffraction pattern. For the *FOX* calculations, information about the numbers of unique P and Al sites, and the oxygen coordination number of P obtained from NMR was used.

The initial structures obtained by *FOX* were further refined with the Rietveld refinement technique using the *RIETAN-FP* program (Izumi & Momma, 2007). For the profile function, the split pseudo-Voigt function of Toraya (1990) was adopted. Diffraction by the glass capillary sample holder gave a complex background shape, especially at lower angles. In order to fit this background well, a composite background function in RIETAN-FP, which is the product of Legendre polynomials and a user-supplied background intensity profile, was used. To obtain the latter, the background in the diffraction pattern was manually fitted by a spline function using the *Fityk* program (Wojdyr, 2010). This procedure improved the fitting at lower angles. Owing to the coexistence of minor phases in the samples (also observed by NMR), trolleite and corundum were also included for the Rietveld refinement of sample #080927B (6 GPa, 1523 K), and corundum and Pt (contamination from the capsule) were included for sample #081113 (7 GPa, 1773 K). Structural parameters of trolleite were taken from Moore & Araki (1974). For these minor phases, no structural parameters except lattice parameters were refined. For sample #080927B (6 GPa, 1523 K), several minor peaks that are unindexed by any known phases and distinctly broader than those of the dominant $AlPO_4$ phase also occur at lower angles. These peaks likely belong to phase(s) with low crystallinity, and could correspond to the unknown phosphate phase(s) revealed by ^{31}P NMR. The regions around these peaks (8.70–9.30, 12.80–13.70 and 15.00–15.70°) were excluded from the Rietveld refinement.

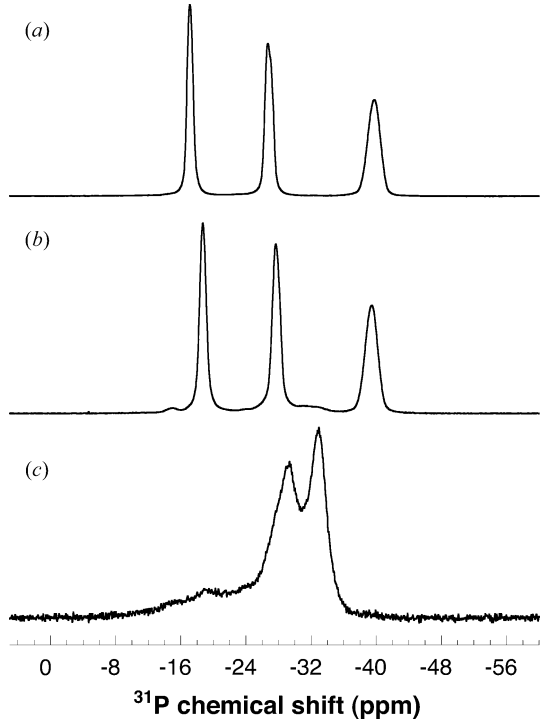

Figure 1
^{31}P MAS NMR spectra for (*a*) sample #081113 (7 GPa, 1773 K) and (*b*) #080927B (6 GPa, 1523 K), both acquired at a spinning speed of 30 kHz, a $\pi/2$ pulse of 2.2 µs and a recycle delay of ∼ 400–700 s ($> 5T_1$) with 87–133 scans averaged. Also shown in (*c*) is the ^{1}H–^{31}P CP-MAS NMR spectrum for sample #080927B acquired at a spinning speed of 30 kHz, a contact time of 8 ms and a recycle delay of 10 s with 2000 scans averaged. All the spectra have been plotted with the same maximum height.

3. Results and discussion

3.1. ^{31}P, ^{1}H MAS NMR and ^{1}H–^{31}P CP-MAS NMR

The ^{31}P MAS NMR spectrum for sample #080927B (6 GPa, 1523 K) contains three main peaks near −18.7, −27.7 and −39.4 p.p.m. with equal integrated intensity, and several very weak peaks near −15, −24 and −32 p.p.m. (broad) (Fig. 1*b*, Table 2). Two-dimensional ^{31}P dipolar double-quantum (DQ)–single quantum (1Q) correlation experiments (using the POST-C7 sequence) have confirmed that the three main peaks belong to a single phase (with cross peaks among all three frequencies; see Xue & Kanzaki, 2010, 2011). These peaks may be attributed to the dominant $AlPO_4$ phase, suggesting that this phase most likely has three P sites of equal population. All three peaks fall within the chemical shift range for four-coordinated P (MacKenzie & Smith, 2002; Stebbins *et al.*, 2009). The varying full-widths-at-half-maximum (FWHM) of the three peaks (1.0–1.8 p.p.m., see Table 2) have been confirmed to result at least partly from ^{27}Al–^{31}P *J* coupling (Xue & Kanzaki, 2011). The presence of weak additional peaks in the ^{31}P MAS NMR spectrum suggests the occurrence of other minor coexisting P-containing phase(s).

In order to further characterize the nature of the observed peaks, ^{1}H–^{31}P CP-MAS NMR spectra were also acquired for sample #080927B (Fig. 1*c*). The spectra contain two peaks near −29.3 and −32.9 p.p.m. and some weaker intensities at higher frequencies, but show no significant intensities near the positions for the three main peaks of the ^{31}P MAS NMR spectrum. The latter is consistent with the anhydrous nature of the dominant $AlPO_4$ phase. The pair of ^{31}P peaks near −29.3 and −32.9 p.p.m. has also been observed, in an intensity ratio of 1:2, in the ^{31}P MAS NMR and ^{1}H–^{31}P CP-MAS NMR spectra (with higher relative intensities in the latter) for other samples synthesized at 6 GPa and 1273 K (#080707) to 1773 K (#080709) using undried $AlPO_4$ as the starting material (see Fig. S1 of the supplementary material), as well as a sample (#091012) synthesized at 5 GPa and 1273 K for 1 h using a starting material of 3 $AlPO_4$ + $Al(OH)_3$ (not shown). The two ^{31}P peaks have been confirmed to correspond to a ^{1}H MAS NMR peak near 4.3 p.p.m. by a two-dimensional ^{1}H–^{31}P HETCOR experiment (see Fig. S2 of the supplementary material). They are most likely due to trolleite that was also revealed by X-ray diffraction. It is worth mentioning that the ^{31}P peak widths for trolleite are systematically narrower (and better resolved) for samples synthesized at the lower temperature of 1273 K (see Fig. S1 of the supplementary material). This suggests that either trolleite possesses a varying degree of disorder depending on temperature or it could have formed from hydrous melt during quench for samples synthesized at higher temperatures ($\geq$ 1523 K). In trolleite, there are two four-coordinated P sites with a 1:2 population ratio, and two H sites with relatively weak hydrogen bonding (O—H···O distances of 3.11 to 3.32 Å; Moore & Araki, 1974). The two

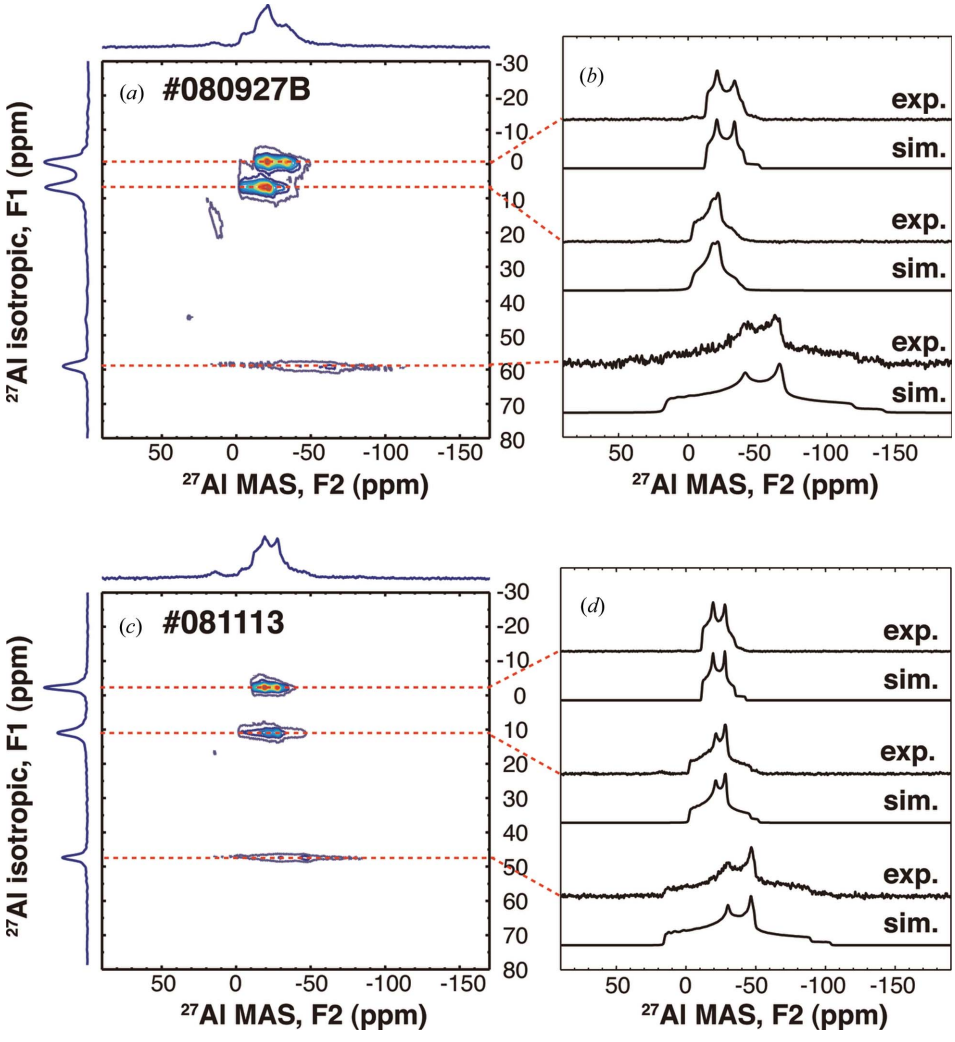

Figure 2
Rotor-synchronized ^{27}Al 3Q MAS NMR spectra with total projections along both dimensions for (*a*) sample #080927B (6 GPa, 1523 K) and (*c*) #081113 (7 GPa, 1773 K), both acquired at a spinning rate of 30 kHz, a recycle delay of 20–25 s (with one steady-state scan before each acquisition), a t_1 time increment of one rotor period (33 µs) and 80–128 t_1 increments (160–256 FID); 48 scans were averaged for each. The contours have been plotted with a linear intensity scale from 5% to 95% in increments of 10%. Also shown in (*b*) and (*d*) are the MAS cross sections and the respective simulated spectra for the three main isotropic peaks (as labelled) for each $AlPO_4$ phase. All the cross sections have been plotted with the same maximum height.

Table 3
^{27}Al NMR results.

Al site†	$F1$ shift (p.p.m.)‡	δ_i^{Al} (p.p.m.)	C_Q^{Al} (MHz)	η_Q^{Al}	T_1^{Al} (s)§
$AlPO_4$ ($P\bar{1}$)					
Al1(Al^{VI})	−0.5	−10.4 (0.3)	5.45 (0.03)	0.34 (0.02)	17 (1)
Al3 (Al^{VI})	7.0	−2.6 (0.3)	5.00 (0.03)	0.75 (0.02)	
Al2 (Al^{V})	59.4	19.0 (0.5)	10.4 (0.1)	0.68 (0.03)	
$AlPO_4$ ($P2_1/c$)					
Al1(Al^{VI})	−2.0	−10.0 (0.3)	4.82 (0.02)	0.44 (0.02)	14 (1)
Al3 (Al^{VI})	11.3	−1.7 (0.3)	5.82 (0.02)	0.72 (0.02)	
Al2 (Al^{V})	47.7	17.0 (0.3)	9.00 (0.02)	0.72 (0.02)	

† Site numbering corresponds to that for crystallographic sites and is assigned according to the two-dimensional through-bond ^{27}Al–^{31}P 3Q-J-HETCOR experiment (see Xue & Kanzaki, 2010, 2011). ‡ $F1$ peak position in the two-dimensional 3Q MAS NMR spectrum at a magnetic field of 9.4 T. § T_1 derived from the one-dimensional MAS NMR spectrum for overlapping peaks.

H sites are unresolved by ^{1}H MAS NMR possibly because of their similar (and weak) hydrogen bonding, as the ^{1}H chemical shift is known to show an inverse correlation with the hydrogen-bonding distance for moderate to strong hydrogen bonding, but show relatively small variations for very weak hydrogen bonding (Xue & Kanzaki, 2009). Similarly unresolved ^{1}H MAS NMR peaks for two proton sites of similarly weak hydrogen bonding have also been previously reported for condrodite-OH ($Mg_5Si_2O_8(OH)_2$) and topaz-OH ($Al_2SiO_4(OH)_2$) (*cf.* Xue & Kanzaki, 2009).

The weak, broad envelope near −32 p.p.m. in the ^{31}P MAS NMR spectrum of sample #080927B (Fig. 1*b*) can only be partially accounted for by the presence of trolleite. A remaining component near −31 p.p.m. (in between the two peak maxima for trolleite) and the two other weak peaks near −15 and −24 p.p.m. must be due to other minor unidentified (mostly likely anhydrous) phosphate phase(s), which may correspond to the weak unindexed peaks in the powder XRD pattern.

The ^{31}P MAS NMR spectrum of sample #081113 (7 GPa, 1773 K) similarly contains three peaks near −17.1, −26.7 and −39.8 p.p.m. with equal integrated intensity (Fig. 1*a*, Table 2). Like the above sample, the two-dimensional ^{31}P DQ–1Q correlation experiment has confirmed that the three peaks belong to a single phase (the dominant $AlPO_4$ phase).

3.2. ^{27}Al MAS and 3Q MAS NMR, and ^{1}H–^{27}Al CP-MAS NMR

The ^{27}Al MAS NMR spectra for both samples contain (partially) overlapping MAS patterns (see Figs. S3 and S4 of the supplementary material). In order to better resolve the different components, two-dimensional rotor-synchronized ^{27}Al 3Q MAS NMR spectra have been obtained for both samples (Figs. 2*a* and *c*). The total projection to the MAS ($F2$) dimension (see Figs. 2*a* and *c*), like the one-dimensional MAS NMR spectra, is broadened by second-order quadrupolar coupling. On the other hand, the isotropic ($F1$) dimension is free from second-order quadrupolar broadening, and clearly reveals the presence of different crystallographically unique Al sites. For both samples, the total projection to the isotropic dimension contains three main peaks, near −0.5, 7.0 and 59.4 p.p.m. (with a relative integrated intensity of 1:1:0.43) for sample #080927B, and near −2.0, 11.3 and 47.7 p.p.m. (with a relative integrated intensity of 1:1:0.6) for sample #081113 (see Fig. 2). The attribution of the three main ^{27}Al isotropic peaks in each sample to a single phase (the respective $AlPO_4$ phase) has been confirmed by high-resolution two-dimensional ^{27}Al–^{31}P dipolar 3Q-HETCOR spectra (that show nine cross peaks among all three ^{27}Al and all three ^{31}P peaks for each sample; see Xue & Kanzaki, 2010, 2011).

The MAS cross section for each of the isotropic peaks in the ^{27}Al 3Q MAS NMR spectra can be reasonably well simulated by a single typical MAS pattern (see Figs. 2*b* and *d*). The resultant ^{27}Al isotropic chemical shift (δ_i^{Al}), quadrupolar coupling constant (C_Q^{Al}) and electric field gradient (EFG) asymmetry parameter (η_Q^{Al}) are tabulated in Table 3. The ^{27}Al isotropic chemical shifts obtained are −10.4, −2.6 and 19.0 p.p.m. for the $AlPO_4$ phase in #080927B, and −10.0, −1.7 and 17.0 p.p.m. for the $AlPO_4$ phase in #081113. The former two peaks of each phase (−10.4 to −1.7 p.p.m.) fall into the chemical shift range for six-coordinated Al (Al^{VI}) and the last (17–19 p.p.m.) matches well with those of five-coordinated Al (Al^{V}) in aluminophosphates (MacKenzie & Smith, 2002). As described below, the former phase is isostructural to $AlVO_4$ and an NMR spectroscopic study of this compound has been reported by Nielsen *et al.* (2002). The reported ^{27}Al isotropic chemical shifts for the three Al sites in $AlVO_4$ (−8.9, −1.1 and 27.2 p.p.m.) are consistent with those of the $AlPO_4$ phase from the present study. The C_Q^{Al} for the five-coordinated Al site (9–10.4 MHz) are significantly larger than those of the two six-coordinated Al sites (4.8–5.8 MHz) for both $AlPO_4$ phases (see Table 2). It is well known that the efficiency for the excitation of 3Q coherence and its subsequent conversion to 1Q or 0Q coherence is strongly dependent on C_Q and becomes less effective for large C_Q (Amoureux, Fernandez & Frydman, 1996). This may explain the apparently lower integrated intensity for the former than the latter two for both phases (whereas all three sites are expected to have equal abundance). In fact, the more quantitative one-dimensional ^{27}Al MAS NMR spectra can be reasonably well simulated with three Al sites of equal abundance using NMR parameters derived above (see Figs. S3 and S4 of the supplementary material).

For other samples synthesized at 6 GPa and 1273 K (#080707) to 1773 K (#080709) using undried $AlPO_4$ as the starting material, as well as a sample (#091012) synthesized at 5 GPa and 1273 K using a starting material of $3AlPO_4 + Al(OH)_3$ (that all contain more abundant trolleite as described above), ^{1}H–^{27}Al CP-MAS NMR and two-dimensional HETCOR spectra revealed a narrower ^{27}Al component with a maximum near −4.1 p.p.m. and a broader component at lower frequency (see Fig. S5 of the supplementary material). These correlate with a ^{1}H peak near 4.3 p.p.m. (for trolleite) and thus most likely correspond to the two six-coordinated Al sites in trolleite (Moore & Araki, 1974). These peaks would partially overlap with peaks for the six-coordinated Al sites of the main $AlPO_4$ phase(s). There-

fore, the ^{27}Al MAS and 3Q MAS NMR spectra for sample #080927B (that was revealed to contain minor trolleite from ^{31}P NMR and XRD) may include a minor contribution from trolleite, which would explain the less satisfactory fit of the MAS cross sections (Fig. 2*b*) and one-dimensional MAS NMR spectrum (Fig. S4 of the supplementary material) compared with that of sample #081113 (Fig. 2*d* and Fig. S3 of the supplementary material).

There is also a minor peak in the ^{27}Al MAS and 3Q MAS NMR spectra for both samples (as well as for all other samples synthesized at 6–7 GPa and 1273–1773 K using dried or undried $AlPO_4$ as the starting material) located at 17 p.p.m. (*F*1) and 14 p.p.m. (*F*2) (see Figs. 2*a* and *c*), which may be attributed to the minor coexisting corundum (*cf.* MacKenzie & Smith, 2002). This peak appears more prominent in total projection to the MAS (*F*2) dimension than that in the isotropic (*F*1) dimension (barely visible), because of its smaller second-order quadrupolar peak width (smaller C_Q^{Al} of 2.38 MHz, *cf.* MacKenzie & Smith, 2002) than those of the main peaks. The attribution of this weak peak to the minor Al_2O_3 corundum has also been confirmed from its absence in one-dimensional ^{1}H → ^{27}Al and ^{31}P → ^{27}Al CP-MAS NMR spectra (see Fig. S5 of the supplementary material).

In summary, the NMR results suggest that sample #080927B consists of a dominant $AlPO_4$ phase with minor trolleite, corundum and unidentified phosphate phase(s), whereas sample #081113 consists of another dominant $AlPO_4$ phase and minor corundum. Each $AlPO_4$ phase contains three tetrahedral P sites of equal population and three Al sites (one five-coordinated and two six-coordinated) of equal abundance. The NMR spectra for both phases are similar (but not identical), suggesting local structural similarity around Al and P between the two phases.

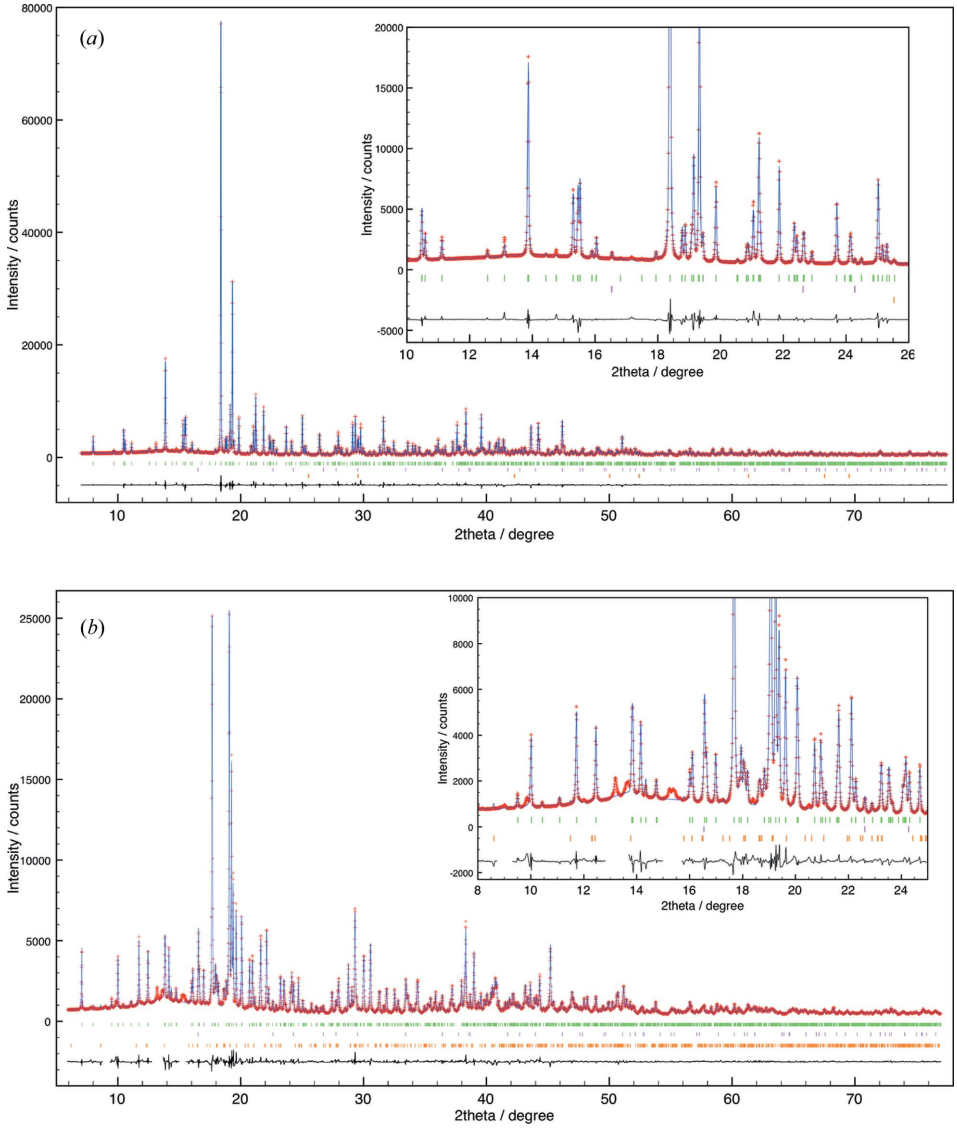

Figure 3
The Rietveld refinement patterns. (*a*) The $P2_1/c$ phase and (*b*) the $P\bar{1}$ phase. The observed intensities are shown by crosses, and the calculated intensities are shown by a line. The line at the bottom is the difference, vertical ticks show positions of reflections. For (*a*) the ticks from top to bottom represent the $P2_1/c$ phase, corundum and Pt. For (*b*) the ticks from top to bottom show the $P\bar{1}$ phase, corundum and trolleite, respectively. Insets show enlarged patterns at low angles. The complex background, prominent in (*b*) at lower angles, is due to diffraction by the glass capillary sample holder. For the $P\bar{1}$ phase (*b*), to exclude peaks due to minor unidentified phase(s), 2θ ranges of 8.70–9.30, 12.80–13.70 and 15.00–15.70° are not used in the refinement.

3.3. Structural analysis by powder X-ray diffraction

The X-ray powder diffraction patterns for both samples were indexed using *TREOR*90 (Werner *et al.*, 1985). A triclinic cell was obtained for the major phase in sample #080927B (6 GPa and 1523 K). The lattice parameters of the phase are a = 6.13283 (10), b = 7.51508 (11), c = 8.58014 (13) Å, α = 98.2630 (7), β = 104.6220 (8), γ = 102.1398 (8)° (values from the Rietveld refinement). A monoclinic cell was obtained for sample #081113 (7 GPa and 1773 K). The lattice parameters of the phase are a = 6.13219 (6), b = 14.34654 (13), c = 8.57620 (9) Å, β = 104.7426 (5)° (values from the Rietveld refinement). The lengths of the a and c axes are very similar for the two phases, suggesting a close structural relationship between them. The number of formulae per unit cell (Z) was estimated as 6 for the triclinic phase, and 12

for the monoclinic phase. The density was calculated as 3.321 (1) g cm^{-3} for the former and 3.3305 (5) g cm^{-3} for the latter. The density difference between the two phases is very small. The densities of the two new high-pressure phases are about 27% higher than that of berlinite, but 4.5% lower than that of the *Cmcm* phase reported by Seifert (1968).

The space group for the new triclinic phase was uniquely identified as $P\bar{1}$, because three independent Al and P sites are identified from the NMR study (as $Z = 6$). This phase is hereafter designated to be the $P\bar{1}$ phase. On the other hand, the space group for the new monoclinic phase could not be uniquely determined at this point and thus all space groups that are consistent with the number of P and Al sites determined from NMR and give low R_{wp} by Le Bail profile fitting ($P2_1/c$, $P2/c$, $P2_1/m$, $P2/m$) were tested in the subsequent structural analysis.

From the ^{31}P MAS NMR study described above, three tetrahedral P sites with equal abundance were identified for both phases. In the modeling using *FOX*, three PO_4 tetrahedra were defined as 'scatterers', and were placed at general positions in the unit cell for both phases. From the ^{27}Al 3Q MAS NMR study, three Al sites were identified. Accordingly, three independent Al atoms were added to the model. Al atoms rather than Al polyhedra were treated here as 'scatterers', because structural solutions can be obtained much faster for the model with Al atoms. This is partly explicable by the smaller number of free parameters for the former model, as each polyhedron has three rotational freedoms whereas an atom has no rotational freedom. In addition, oxygen overlaps between P and Al polyhedra were avoided. A similar observation was reported for an aluminium methylphosphonate (Favre-Nicolin & Černý, 2002). As a result, no constraint was placed on the coordination number of Al during the calculations. Additionally, an '*anti*-bump' cost function implemented in *FOX* was used to avoid improbable configurations. This cost function adds a penalty when two atoms get closer together than a pre-defined minimum distance, and thus helps to obtain the correct structure. The local structural information obtained by NMR helped to set the proper '*anti*-bump' distances. For the $P\bar{1}$ phase the crystal structure was readily obtained from this model. For the monoclinic phase, the structure with the lowest R_{wp} was obtained when the space group $P2_1/c$ was assumed. Hereafter, this phase is designated as the $P2_1/c$ phase. Although no constraint on the oxygen coordination number of Al was given during the *FOX* calculations, the resultant coordination states of the Al sites in these structures are consistent with the ^{27}Al 3Q MAS NMR results.

The initial structures obtained by FOX were then refined using the Rietveld refinement program *RIETAN-FP* (Izumi & Momma, 2007). The final R_{wp} and S for the pattern of sample #080927B were 0.0442 and 1.43, respectively, and the R_I (= R_B) for the $P\bar{1}$ phase was 0.0165. The fitted powder X-ray diffraction pattern of the $P\bar{1}$ phase is shown in Fig. 3(*b*). The final R_{wp} and S for the pattern of sample #081113 were 0.0490 and 1.56, and the R_I for the $P2_1/c$ phase was 0.0212. The fitted powder X-ray diffraction pattern of the $P2_1/c$ phase is shown in Fig. 3(*a*).

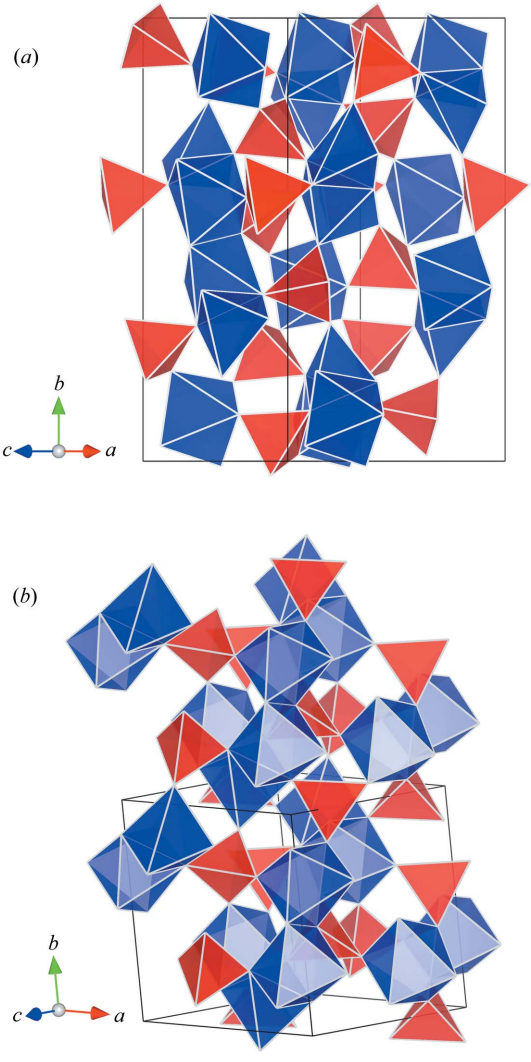

Figure 4
Crystal structures of high-pressure $AlPO_4$ phases. (*a*) The $P2_1/c$ phase and (*b*) the $P\bar{1}$ phase. Red tetrahedra represent the PO_4, whereas blue polyhedra show AlO_5 and AlO_6. Crystal structures are drawn by *VESTA* (Momma & Izumi, 2008).

3.4. Structures of high-pressure $AlPO_4$ phases

The structures of the two phases are shown in Fig. 4. As noted below, the $P\bar{1}$ phase is isostructural to $FeVO_4$ and $AlVO_4$, and the cation site labeling of $FeVO_4$ used by Robertson & Kostiner (1972) is followed. Owing to their similarity in local structure, each site corresponding to that in the $P\bar{1}$ phase with the same local structure (first nearest neighbors) is identified in the $P2_1/c$ phase, and the same site labeling is adapted. This facilitates easy comparison of the corresponding bond distances. Both phases contain one five-coordinated (Al2) and two octahedral Al (Al1 and Al3) sites. The five-coordinated Al is in a distorted bipyramidal configuration. As shown in Fig. 5 a doubly bent chain made of six edge-shared Al polyhedra in the order Al1–Al2–Al3–Al3–Al2–Al1 is recognized in both phases. A center of symmetry is located at the center of this chain. The short chains are

Table 4
Selected bond distances (Å) of the $P\bar{1}$ $AlPO_4$ phase.

P1—O11	1.499 (4)	Al1—O12	2.077 (5)
P1—O12	1.595 (4)	Al1—O14	1.822 (4)
P1—O13	1.614 (3)	Al1—O22	1.804 (4)
P1—O14	1.529 (4)	Al1—O23	1.813 (5)
P2—O21	1.594 (4)	Al1—O24	2.050 (4)
P2—O22	1.538 (4)	Al1—O34	1.859 (5)
P2—O23	1.512 (3)	Al2—O12	1.822 (5)
P2—O24	1.592 (4)	Al2—O13	1.963 (5)
P3—O31	1.632 (4)	Al2—O24	1.841 (4)
P3—O32	1.549 (4)	Al2—O31	1.831 (5)
P3—O33	1.524 (4)	Al2—O32	1.718 (5)
P3—O34	1.472 (4)	(Al2—O21	3.206 (4))
		Al3—O11	1.774 (4)
		Al3—O13	1.828 (5)
		Al3—O21	1.817 (4)
		Al3—O21	2.108 (4)
		Al3—O31	1.948 (5)
		Al3—O33	1.776 (5)

Table 5
Selected bond distances (Å) of the $P2_1/c$ $AlPO_4$ phase.

P1—O11	1.507 (4)	Al1—O12	2.012 (4)
P1—O12	1.583 (4)	Al1—O14	1.886 (4)
P1—O13	1.592 (4)	Al1—O22	1.824 (4)
P1—O14	1.509 (3)	Al1—O23	1.831 (4)
P2—O21	1.582 (4)	Al1—O24	2.035 (4)
P2—O22	1.489 (4)	Al1—O34	1.835 (4)
P2—O23	1.532 (4)	Al2—O12	1.880 (4)
P2—O24	1.585 (4)	Al2—O13	1.918 (4)
P3—O31	1.653 (3)	Al2—O24	1.794 (4)
P3—O32	1.566 (4)	Al2—O31	1.834 (4)
P3—O33	1.534 (3)	Al2—O32	1.700 (4)
P3—O34	1.501 (4)	(Al2—O14	3.078 (3))
		Al3—O11	1.777 (4)
		Al3—O13	1.881 (4)
		Al3—O21	1.833 (4)
		Al3—O21	2.167 (4)
		Al3—O31	1.984 (4)
		Al3—O33	1.750 (4)

connected to one another by PO_4 tetrahedra to form a three-dimensional network structure. This structure is in contrast to that of the *Cmcm* phase ($CrVO_4$), which consists of infinite straight chains made of edge-shared octahedral Al. The structural differences between the $P\bar{1}$ and $P2_1/c$ phases are compared in Fig. 5. In the $P\bar{1}$ phase, only a single type of orientation of the chains exists (Fig. 5*b*), whereas two alternate orientations exist in the $P2_1/c$ phase (Fig. 5*a*). This structural difference suggests that the transition from the $P\bar{1}$ to $P2_1/c$ phase is reconstructive.

Selected bond distances for the $P\bar{1}$ and $P2_1/c$ phases are shown in Tables 4 and 5. As mentioned above, the corresponding bond distances can be directly compared between the two phases. Good correlation in bond lengths between the two phases is observed. The P—O distances show a bimodal distribution in both phases, and the variation is rather large (1.472–1.632 Å for the $P\bar{1}$ phase; 1.489 to 1.653 Å for the $P2_1/c$ phase). The longest two (1.632 and 1.653 Å) are beyond the known P—O distance variation in PO_4 tetrahedra observed in minerals (1.439–1.625 Å; Huminicki & Hawthorne, 2002). There are two types of oxygen sites in these structures, one is coordinated with one Al and one P, and the other is coordinated by two Al and one P. Therefore, the oxygen sites are either under-bonded or over-bonded, with the latter corresponding to longer P—O bond distances, thus explaining the bimodal distribution of P—O distances. The longest P—O distance is from the most over-bonded oxygen site, O31, which is coordinated with a five-coordinated Al (Al2), an octahedral Al (Al3) and a P (P3). In order to check whether five-coordinated Al is intrinsic or remnant of originally six-coordinated Al distorted during decompression, the distance between the five-coordinated Al (Al2) and the sixth nearest oxygen for each phase is also listed in Tables 4 and 5. These distances are over 3.0 Å. If the Al octahedron is assumed to be formed by the sixth oxygen, it would share an edge with a PO_4 tetrahedron, which is energetically unfavorable. Therefore, the local structural configuration suggests that the five-coordinated Al observed in the two high-pressure phases is intrinsic.

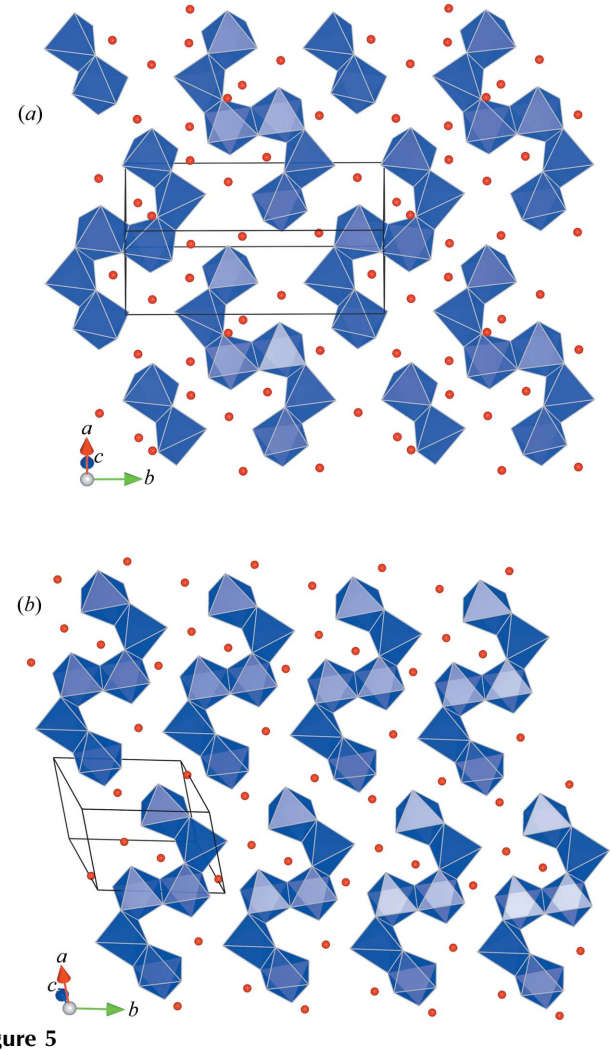

Figure 5
A layer made of Al-polyhedral chains in the $AlPO_4$ phases [parallel to the ($\bar{1}02$) plane]. (*a*) The $P2_1/c$ phase and (*b*) the $P\bar{1}$ phase. These layers are jointed by the tetrahedral PO_4 forming a three-dimensional network structure. The small red spheres are P atoms. For clarity, the PO_4 tetrahedra are not shown. All chains with the same orientation can be seen in the $P\bar{1}$ phase (*b*), whereas chains with two alternative orientations are recognized for the $P2_1/c$ phase (*a*).

Table 6
Comparison of lattice parameters for the $P\bar{1}$ ABO_4 phases.

Formulae	a (Å)	b (Å)	c (Å)	α (°)	β (°)	γ (°)
$AlPO_4$†	6.13283 (10)	7.51508 (1)	8.58014 (13)	98.2630 (7)	104.6220 (8)	102.1398 (8)
$AlVO_4$‡	6.538 (2)	7.756 (3)	9.131 (3)	96.17 (7)	107.23 (8)	101.40 (9)
$FeVO_4$§	6.719 (7)	8.060 (9)	9.254 (9)	96.65 (8)	106.57 (8)	101.60 (8)

† Present study. ‡ Arisi *et al.* (2004). § Robertson & Kostiner (1972).

After the refinements were completed it was apparent that the $P\bar{1}$ phase is isostructural with $FeVO_4$ (Robertson & Kostiner, 1972) and $AlVO_4$ (Arisi *et al.*, 2004), which are stable at ambient pressure. The lattice parameters of the $P\bar{1}$ ABO_4 structure are compared in Table 6. In $AlVO_4$ the same doubly bent Al polyhedra chains exist, whereas in $FeVO_4$ the chains are made of Fe polyhedra. The corresponding $P2_1/c$ polymorph as found for $AlPO_4$ in the present study might be expected for $FeVO_4$ or $AlVO_4$ at high temperature, although no such phases have been reported to date.

There have been several attempts to systematically classify crystal structures in the ABX_4 system using ionic radii (Seifert, 1968; Fukunaga & Yamaoka, 1979; Bastide, 1987; Errandonea & Manjón, 2008). Seifert (1968) classified the crystal structures based on a plot of r_A/r_X *versus* r_B/r_X. A similar plot (with $r_A > r_B$) was proposed by Bastide (1987) and used to explain and predict pressure-induced phase-transformation sequences. Owing to greater compressibility for the larger anion, a higher-pressure phase is expected with increasing r_A/r_X and increasing r_B/r_X (*i.e.* NE direction in Bastide's figure). Errandonea & Manjón (2008) presented an updated version of Bastide's plot, and using this, both the $P\bar{1}$ phase ($FeVO_4$ and $AlVO_4$) and the *Cmcm* phase ($CrVO_4$) are expected high-pressure phase(s) of $AlPO_4$. Our finding of the $P\bar{1}$ phase as a high-pressure form of $AlPO_4$ is in accordance with this prediction. However, the $P2_1/c$ phase (and the $P2/c$ phase described below) could not be predicted from the plot, as no corresponding phase was known. This demonstrates the limited predictive ability based on such empirical approaches.

Very recently we found yet another new $AlPO_4$ phase with space group $P2/c$ at 5 GPa and 1273 to 1773 K (Kanzaki & Xue, unpublished). In this phase, P and Al are all in tetrahedral coordination. On the other hand, at 10 GPa and 1273 K we observed the *Cmcm* phase, consistent with the studies by Seifert (1968) and Stebbins *et al.* (2009). Therefore, the phase transition sequence of $AlPO_4$ with pressure up to 18 GPa is as follows [with coordination number of Al site(s) in parenthesis]: berlinite (Al^{IV}) → $P2/c$ phase (Al^{IV}) → $P\bar{1}$ phase ($1Al^{V}$, $2Al^{VI}$)/$P2_1/c$ phase ($1Al^{V}$, $2Al^{VI}$) → *Cmcm* phase (Al^{VI}). This sequence is quite different from that derived from the DAC studies mentioned in §1 (*e.g.* Pellicer-Porres *et al.*, 2007). As DAC is generally conducted at room temperature, this precludes the observation of reconstructive-type phase transitions which have high thermal activation energies. In order to fully understand the structural chemistry of the ABO_4 system, it is important to conduct experiments at both high temperature and high pressure. Our findings suggest there may yet be unexplored ABO_4 phases.

The present study has demonstrated the usefulness of the combined application of *ab initio* structure determination from powder X-ray diffraction and solid-state NMR spectroscopy for the structural characterization of high-pressure samples. Recent progress in high-resolution solid-state NMR techniques renders information about the number of sites and their coordination numbers readily obtainable not only for spin $\frac{1}{2}$ nuclei such as ^{31}P, but also for traditionally more difficult quadrupole nuclei such as ^{27}Al (*e.g.* MacKenzie & Smith, 2002). Such local structural information can be most efficiently utilized with *ab initio* structure analysis programs like *FOX*, which incorporates polyhedral units (or partial structure) in the structural model. Solid-state NMR is also ideal for revealing any disordered distribution of cations or anions (*e.g.* Xue *et al.*, 2010). Therefore, the combined application of *ab initio* structure determination *via* X-ray powder diffraction and solid-state NMR is becoming a powerful technique allowing the rapid solution of complex inorganic crystal structures.

We would like to thank two anonymous reviewers and the editor (Dr T. J. White) for constructive comments. We are also grateful to Dr Ken-ichi Funakoshi for permission to use the SPEED1500 press, to Dr Keiichi Osaka for assistance with the Debye–Scherrer camera measurement at SPring-8, and to Dr Y. Yachi for help during preliminary synthesis experiments at ISEI. This study was supported by Grants-in-Aid for Scientific Research funded by the Ministry of Education, Culture, Sports, Science and Technology of Japan. Part of this work was carried out during the Misasa International Student Intern Program (MISIP) 2008 (SR) and 2009 (EB and SN).

References

Amoureux, J.-P. & Fernandez, C. (1998). *Solid State Nucl. Magn. Reson.* **10**, 211–223.
Amoureux, J.-P., Fernandez, C. & Frydman, L. (1996). *Chem. Phys. Lett.* **259**, 347–355.
Amoureux, J.-P., Fernandez, C. & Steuernagel, S. (1996). *J. Magn. Res. A*, **123**, 116–118.
Arisi, E., Oalomares Sánchez, S. A., Leccabue, F., Watts, B. E., Bocelli, G., Calderón, F., Calestani, G. & Righi, L. (2004). *J. Mater. Sci.* **39**, 2107–2111.
Bass, J. D. & Sclar, C. B. (1979). *Am. Mineral.* **64**, 1175–1183.
Bastide, J. P. (1987). *J. Solid State Chem.* **71**, 115–120.
Dachille, F. & Roy, R. (1959). *Z. Kristallogr.* **111**, 451–461.
Errandonea, D. & Manjón, F. J. (2008). *Prog. Mater. Sci.* **53**, 711–773.
Favre-Nicolin, V. & Černý, R. (2002). *J. Appl. Cryst.* **35**, 734–743.
Fukunaga, O. & Yamaoka, S. (1979). *Phys. Chem. Miner.* **5**, 167–177.
Gillet, P., Badro, J., Varrel, B. & McMillan, P. F. (1995). *Phys. Rev. B*, **51**, 11262–11269.
Hemley, R. J., Jephcoat, A. P., Mao, H. K., Ming, L. C. & Manghnani, M. H. (1988). *Nature*, **334**, 52–54.

Huminicki, D. M. C. & Hawthorne, F. C. (2002). *Phosphates – Geochemical, Geobiological, and Materials Importance*, edited by M. J. Kohn, J. Rakovan & J. M. Hughes, pp. 123–253. Washington, DC: Mineralogical Society of America.
Izumi, F. & Momma, K. (2007). *Solid State Phenom.* **130**, 15–20.
Kanzaki, M. (1992). *High Temp. High Pressures*, **24**, 519–523.
Kanzaki, M. (2010). *Am. Mineral.* **95**, 1349–1352.
Kruger, M. B. & Jeanloz, R. (1990). *Science*, **249**, 647–649.
MacKenzie, K. J. D. & Smith, M. E. (2002). *Multinuclear Solid-State NMR of Inorganic Materials*. Amsterdam: Pergamon Press.
Momma, K. & Izumi, F. (2008). *J. Appl. Cryst.* **41**, 653–658.
Moore, P. B. & Araki, T. (1974). *Am. Mineral.* **59**, 974–984.
Nielsen, U. G., Boisen, A., Brorson, M., Jacobsen, C. J. H., Jakobsen, H. J. & Skibsted, J. (2002). *Inorg. Chem.* **41**, 6432–6439.
Nishibori, E., Takata, M., Kato, K., Sakata, M., Kubota, Y., Aoyagi, S., Kuroiwa, Y., Yamakata, M. & Ikeda, N. (2001). *Nucl. Instrum. Methods Phys. Res. A*, **467–468**, 1045–1048.
Pellicer-Porres, J., Saitta, A. M., Polian, A., Itié, J. P. & Hanfland, M. (2007). *Nature Mater.* **6**, 698–702.
Robertson, B. & Kostiner, E. (1972). *J. Solid State Chem.* **4**, 29–37.
Seifert, K.-F. (1968). *Fortschr. Miner.* **45**, 214–280.
Sharan, B. & Dutta, B. N. (1964). *Acta Cryst.* **17**, 82–85.
Sharma, S. M., Garg, N. & Sikka, S. K. (2000). *Phys. Rev. B*, **62**, 8824–8827.
Stebbins, J. F., Kim, N., Brunet, F. & Irifune, T. (2009). *Eur. J. Mineral.* **21**, 667–671.
Toraya, H. (1990). *J. Appl. Cryst.* **23**, 485–491.
Utsumi, W., Funakoshi, K., Urakawa, S., Yamakata, S., Tsuji, K., Konishi, H. & Shimomura, O. (1998). *Rev. High Pressure*, **7**, 1484–1486.
Werner, P.-E., Eriksson, L. & Westdahl, M. (1985). *J. Appl. Cryst.* **18**, 367–370.
Wojdyr, M. (2010). *J. Appl. Cryst.* **43**, 1126–1128.
Xue, X. & Kanzaki, M. (2009). *J. Am. Ceram. Soc.* **92**, 2803–2830.
Xue, X. & Kanzaki, M. (2010). *Proc. Soc. Solid State NMR Mater.* **47**, 9–12.
Xue, X. & Kanzaki, M. (2011). In preparation.
Xue, X., Kanzaki, M. & Fukui, H. (2010). *Am. Mineral.* **95**, 1276–1293.